University of Twente.
Energy, Materials and Systems (EMS)
Faculty of Science and Technology (TNW)

Experimental and modelling studies of transverse load on DI-BSCCO tapes

Master Thesis

Bas Pellen

September 30, 2021

Supervised by:

Dr. Ing. A Nijhuis
Ing. R. Lubkemann

Committee members:

Professor/chair	Prof. Dr. Ir. H.J.M. ter Brake
Supervisor	Dr. Ing. A Nijhuis
Reference member	Dr. A. van Houselt

Abstract

The Flutter coil for Varian's next generation proton therapy treatment facility, uses DI-BSCCO high temperature superconducting tapes. The coil under full load experiences a large transverse force. In this thesis, the transverse load limits of the tape are experimentally tested, showing irreversibly degradation around $-250\,\mathrm{MPa}$ when pressing with a 1 mm pushing head. This is compared with a 3D simulation of the experiment, where a BSCCO filament failure criterion of $\sigma_3 = -775\,\mathrm{MPa}$ shows the same degradation as the experiment. A single tape inside the coil is then modeled and this shows that the transverse load limit of the Flutter coil under full load amounts to $-600\,\mathrm{MPa}$, which means a safety margin of approximately 300%.

Contents

1 | Introduction

One of the techniques to treat cancer is with proton therapy. Varian delivers full proton therapy solutions. To make those systems available to a larger sales market, the system has to be reduce in size and cost [1]. An impression of the potential reduction in size and weight, through the use of superconductors can be seen in figure 1.1.

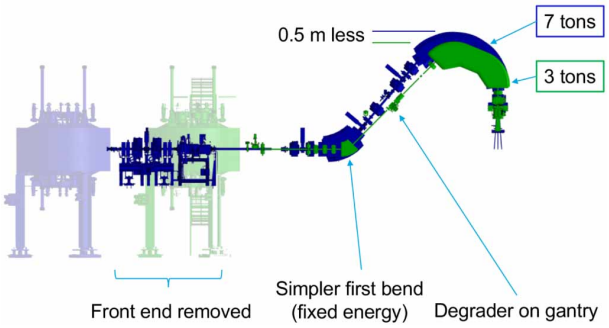

Figure 1.1: Artistic impression of potential size reduction when using superconductors. [1]

A part of this system is the cyclotron, which accelerates the protons up to 250 MeV. Varian's AC250 isochronous superconducting cyclotron is shown in figure 1.2. This cyclotron has iron pieces to focus the magnetic field, which is needed to focus the particle beam. When the size of the cyclotron is decreased the field generated by the main coils has to increase, to be able to accelerate the protons up to the same energy levels. With these higher fields, the iron will saturate and the effect of these iron 'flutter' pieces will be limited. Therefore superconducting Flutter coils will need to replace the iron pieces, which create the flutter field.

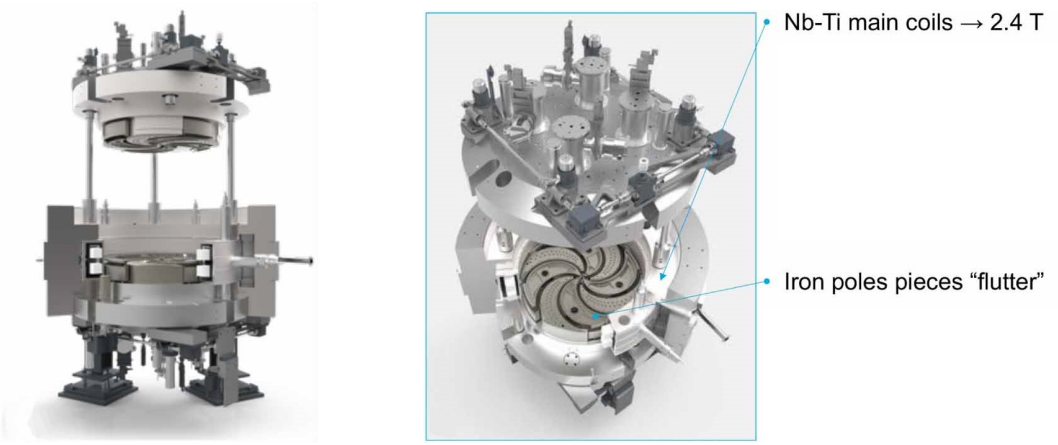

(a) (b)

Figure 1.2: Artistic impression of Varian's AC250 isochronous superconducting cyclotron. [1] (a) Side view (b) Top view, where the iron pieces which generate the flutter field are visible.

The Flutter coils are produced by Sumitomo Electric Industries and the coils are fabricated from their DI-BSCCO Bi-2223 conductor. The Flutter coil consists of 6 double pancakes, which are shaped in the form of a kidney. A proof of concept coil can be seen in figure 1.3.

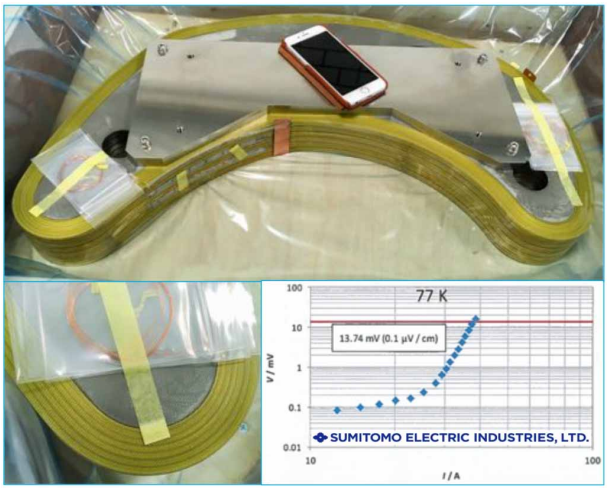

Figure 1.3: Flutter coil. [1]

Due to the shape of the coil, the transverse stress in the coil can become very high. To ensure that the coil will not fail under normal operating conditions, due to these transverse loads, the study in this thesis is conducted.

First some experiments are performed on the DI-BSCCO tapes. The experiments are performed at 77 K, where the tapes are subjected to a transverse load. The experiment is then simulated in COMSOL Multiphysics® [2], where a 3D model is made of the experiment. This is purely a mechanical model and the goal is to find a failure criterion of the BSCCO filaments. The way this is done, is by comparing the percentage of BSCCO which has not reached this criterion, with the degradation curve of the experimental data.

The 3D model approximates the silver matrix and the BSCCO filaments as one material, with the rule of mixtures. The use of this approximation needs to be validated and this is

done in 2D COMSOL Multiphysics® simulations.

When the failure criterion is determined and the rule of mixtures approximation has been validated, the failure criterion can be used to analyze the mechanical stability of the Flutter coil. This is done by modeling a single tape in 2D space, where it is encapsulated in epoxy.

This thesis will first explain key concepts in chapter 2, then it will explain how the experiments are performed in chapter 3. The different models will be explained in chapter 4 and the results of the experiments and models will be shown and discussed in chapter 5. A conclusion of this work will be drawn in chapter 6 and finally some recommendations will be made for future work in chapter 7.

2 | Theory

2.1 Superconductivity

Conductors used to have a finite resistance, until the 8th of April in 1911, when Heike Kamerlingh Onnes made the discovery[1] that makes today's superconducting applications possible [3]. This discovery was that some materials, that are now called superconductors, have no resistance when cooled bellow a certain temperature. This has several advantages to normal conductors.

One is that no energy is being dissipated in the form of heat when current is passed through the superconductor. This means that the only price in terms of energy that is being paid, is the energy which is needed to cool the superconductor down and the energy needed to keep it cold. An exception to this is alternating current, however this is irrelevant to this work.

Another advantage is that much higher engineering current densities can be achieved compared to normal conductors. This is useful for applications where a superconducting coil is used to generate a high magnetic field.

2.1.1 Critical limits of superconductivity

The superconducting state is bound by several parameters. The temperature, magnetic field, current density and strain. They all contribute to the limit of the superconducting state. Once that limit is reached the superconductor will transition from the superconducting state into the normal state.

Critical temperature

The first and one of the most important parameter is the temperature. Technical superconductors will enter the superconducting state at temperatures, which are far below room temperature. There are 2 main categories: Low Temperature Superconductors (LTS) and High Temperature Superconductors (HTS). The low temperature superconductors function at an operating temperature of 4.2 K, which is the temperature of liquid helium. Their critical temperature is a few kelvins above the operating temperature, for stability reasons. This additional margin is called the temperature margin.

The high temperature superconductors are able to operate at 77 K, which is the temperature of liquid nitrogen. As with LTS, the critical temperature lays above this operating temperature of 77 K. Because the HTS is also able to operate at lower temperatures than 77 K, there is a big benefit of using HTS over LTS, which is that a greater temperature margin can be achieved.

[1] As is tradition, I have to include this in my thesis.

Critical magnetic field

The magnetic field in which the superconductor is placed plays a big role in the limits of the superconductor. There are two magnetic field limits. The first one is the point where the superconductor no longer completely expels the magnetic field and that happens at a typical magnitude of a couple of millitesla's. In the region between the first and the second critical magnetic field limit, there are small normal zones in the superconductor which contain magnetic flux. These are called vortices and help balance the magnetic pressure and the superconducting state. Ones the second limit is reached the superconductor leaves the superconducting state completely. Since a lot of superconducting application contain high magnetic fields, the second critical magnetic field is the most important. Depending on the superconductor, the angle of the magnetic field with the superconductor also matters greatly [4].

Critical current density

The critical current depends on the application the superconductor is used for, and the other parameters are tuned to reach this set goal. Therefore it is usual to describe the critical current as a function of the other parameters.

There are a few definitions of critical current or critical current density. One is the critical current inside the superconducting material only. Another is the critical current divided by cut through area of the tape or cable. This is called the critical engineering current density. When the critical current in this thesis is mentioned, it means the amount of current that can pass through the measured superconducting tape, without it leaving the superconducting state. More on this transition in section 2.1.2.

Critical strain

The last critical parameter is critical strain. This is caused by stresses which are put on the superconductor from various forces. Due to deformation of the superconducting material itself, the superconducting properties will degrade. Critical strain will be handled in detail in section 2.2, since it is of great importance to this work.

Quenching

A quench is an undesired phenomenon. It means that the superconductor will sudden and unexpected leave the superconducting state. This will need to be handled properly in order to minimize the damage it can cause to the superconductor or the device of which the superconductor consists of. For short samples tests it is usually not that big of a deal when they burn, however if the superconductor in an application burns, it can become quite costly. Therefore it is best to prevent a quench and/or to be able to dump the energy stored in the system, so that it cannot do any damage.

2.1.2 Power Law

The behavior of a superconductor around the transition regime is described by the power law, which is shown in equation 2.1.

$$\frac{E}{E_c} = \left(\frac{I}{I_c}\right)^n \tag{2.1}$$

In this equation E is the electric field, I is the current through the tape and n is the n-value, which is describing how smooth or sudden the transition is between the superconducting and the normal state. I_c is a parameter which is important, as this indicates where the transition takes place. However, since the transition is smooth, a criterion is needed to

define where I_c is. This criterion is defined by the critical electric field E_c. The E_c criterion used in this work is shown in equation 2.2.

$$E_c = 10\,\mu V m^{-1} \tag{2.2}$$

The n-value is not influenced by the value which is chosen for E_c. However I_c is depended on E_c. Normally it can be converted easily if the n-value is known. So when an $I_c(\sigma)$ is plotted the shape of the curve will stay the same when it is converted to a different E_c criterion when the n-value is constant. However if the n-value is changing because of degradation. The shape of the converted curve will be different and therefore it is important which E_c criterion is chosen when interpreting and comparing data. Sumitomo used a different E_c criterion to measure the performance of their tape, they used a criterion of $E_c = 100\,\mu V m^{-1}$ [5]. The criterion of $E_c = 10\,\mu V m^{-1}$ was chosen over the criterion of $E_c = 100\,\mu V m^{-1}$, because the lower E_c criterion is used for mature HTS conductors.

2.1.3 Four-point measurement

For a proper IV measurement, a four-point measurement has to be conducted [6]. The way this is done is by separating the voltage taps and the current leads. This set-up is shown in figure 2.1.

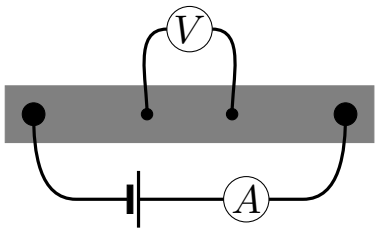

Figure 2.1: Four-point measurement, where voltage taps and current leads have been separated.

This is done to prevent measuring the resistive part of the current lead, so only the voltage over the superconductor will be measured, avoiding a linear component and the IV curve will only follow the power law described by equation 2.1.

2.2 Strain

Stress and strain are related closely. To deform a material, a force is needed. The relation between the stress and strain for most used materials can be found in databases. There are several regimes in this stress strain relation. The first one is the elastic regime. In this regime the Young's modulus determines the relation. The other regime is the plastic regime. In this regime permanent deformation occurs. This means that the structure of the material will permanently deform. In this work stress will be named throughout, since that is the parameter that can be measured directly. However it is the strain that is causing the deformation that leads to degradation of the superconductor.

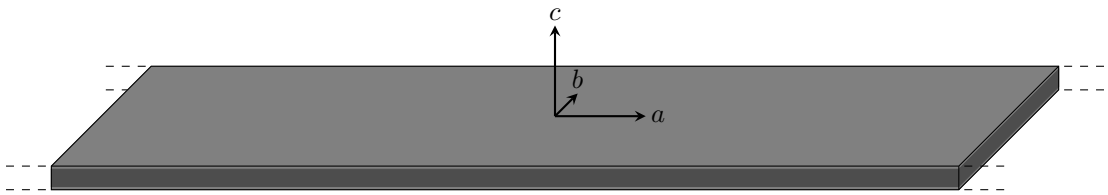

Figure 2.2: Schematic of a section of the tape.

A rough schematic of the tape is shown in figure 2.2. Where the a, b and c axis are along the length, width, and height of the tape respectively. The type and direction of the strain is important for the performance of the superconductor.

2.2.1 Transverse compressive strain

Transverse strain is caused by stress in the transverse direction. In case of the BSCCO tape this is along the c-axis. In 2000 Bray [7] showed that stress levels of 150 MPa could sometimes be reached without degrading the superconductor. According to the specifications[2] of the measured tape, the critical compressive stress in the transverse direction should at least be larger than 150 MPa.

DI-BSCCO Type-H has been used in transverse compressive stress measurements by Ito and Hashizume [8]. The pushing head width was 5 mm and the critical stress that has been found was 220 MPa, which is already higher than the manufacturers specification. The critical strain which corresponds to this stress level is 0.4 %. This is a tape which has not been reinforced with any stainless-steel or copper, so this is purely the strength of the actual superconducting material and its matrix, which is taking the load.

According to Takoa [9] the length over which the pressure is applied matters for the resulting degradation of the tape. Takoa [9] reports that the superconductor will degrade more for a particular stress level when the pushing head is larger. However, no explanation is presented in this work.

The degradation as a result of transverse compressive strain and axial tensile strain has different causes [10] and behave differently [11]. The degradation is also dependent on the initial critical current density. Umekawa [11] showed that both the relative critical current and the relative n-value experience a greater decline when the initial critical current is higher.

2.2.2 Transverse tensile strain

Transverse tensile strain is caused by tensile stress in the transverse direction. In case of the BSCCO tape this is along the c-axis, as shown in figure 2.2.

This type of stress is relevant in epoxy impregnated coils because the epoxy will be attached to the superconductor. This means that if there are Lorentz forces, the tape will be under stress in the transverse direction. Another phenomenon is tensile stresses due to the difference in thermal contraction between the tape and the epoxy. Epoxy will contract more than the superconductor [12], which means that the superconductor can experience an internal tensile stress. Research has shown that the stresses at which the tapes fail, is about an order of magnitude lower [13] than the critical tensile stress in the axial direction. The critical strain at which this failure occurs is around 0.4% [14].

2.2.3 Axial tensile strain

Axial strain is caused by stress in the axial direction, which is along the a-axis as shown in figure 2.2. This is also the most common form of strain on a superconductor. This is due to the fact that superconductors are mostly used to make coils. Inside these coils, the

[2]Confidential document

hoop stresses can rise significantly, and those stresses are mainly axial tensile stresses for the superconductor.

According to the specifications[3] of the measured tape, the critical tensile strain in the axial direction is 0.4% and the critical tensile stress in the axial direction is 270 MPa. The critical strain levels which are found in literature match the manufacturers given strain of 0.4% [15, 16]. Tapes with similar specifications have been tested by Naoki [17] and it was found that the critical axial tensile stress and strain are 310 MPa and 0.42% respectively.

Previous research showed that it is possible to reach higher critical tensile stress levels, namely in the order of 350 MPa, however these were for thicker tapes [18]. It also states that pretension during manufacturing can increase the critical tensile stress. Other recent research [19] shows that for tapes, which have the same thickness as the ones used in this work, the critical tensile stress is 278 MPa and up to 317 MPa when more pretension is applied during manufacturing. All these critical levels are determined at a 99% recovery criterion.

Fatigue loading is an important factor when it comes to the reversibility of the critical current. It has been documented that a steel reinforcement structure greatly increases the life cycle when the conductor is submitted to fatigue loading [20, 21].

2.2.4 Axial compressive strain

Axial compressive strain also acts along the axial direction. For the compression and normalized critical current, the following relation has been found by previous research [22]. This is shown in equation 2.3, where $a = 0.038$ and $b = 1.11$.

$$I_c = 1 - (\epsilon_a / a)^b \tag{2.3}$$

2.2.5 Side compressive strain

The last direction is the side direction, which is along the b-axis as shown in figure 2.2. There is no research found on the strain levels compared to the I_c, however stress dependencies can be found in literature [23]. It has been found that the critical stress highly depends on the thickness of the tape. This is due to irregularities in the tapes, which will result in higher fluctuations in stress levels for smaller tapes. Resulting in a larger degradation of I_c in terms of stress. The critical stress levels for the side compressive stress are similar to the critical stress levels for the transverse compressive stress in the studied literature.

2.3 Mechanical failure and critical current.

Apart from the different strain directions and relations between the critical current and the strain level, the question is: why does the critical current decrease. This happens due to deformation in the lattice structure. Up till a certain point this is reversible, but after that the brittle BSCCO material will crack, or the material will plastically deform. Both phenomena will cause a permanent change in the critical current. Due to the brittle nature of BSCCO the maximum principal stress can predict the fracture probability well [24], which means that when only compressive transverse strain is applied, this theory can directly be linked to the critical current. However, when the length of the pressure area is not long, the shear stresses have a much higher influence on the deformation or damage than when the pressure is being applied over the whole length of the tape [25]. There are ways to prevent this damage from happening and one of these ways is via a steel support structure. This support structure can reduce micro crack formation and growth [20]. Then there is also a difference in the way degradation is caused. Degradation because of transverse compressive strain and axial tensile strain have different causes [10].

[3] Confidential document

To understand what is happening in the simulations, the stresses are mapped to the surfaces of the geometry. These can be described with different definitions, and they are explained in the next subsections.

2.3.1 Cauchy stress

The Cauchy stress is one of the most used stresses. It is defined by the force which act upon an infinitesimal volume element in the deformed body. So, these stresses on the deformed body are described in the reference frame. This is useful for modeling something which is being deformed to see the stresses acting as they deform.

2.3.2 Second Piola–Kirchhoff stress

The Second Piola–Kirchhoff stress is very similar to the Cauchy stress. The difference is that in this case the stress which the deformed body is experiencing is projected back onto the body prior to deformation. These projected stresses are then described in the reference frame.

2.3.3 Principal stress

The Cauchy stress and second Piola–Kirchhoff stress tensors have three normal stresses and six shear stresses. The principal stress is defined in such a way that the shear stresses are zero. This is done by rotating the axis. This leaves three normal stresses, which are also defined in a specific way. Namely: $\sigma_1 \geq \sigma_2 \geq \sigma_3$. So the maximum tensile stress is defined by σ_1 and the maximum compressive stress is defined by σ_3. Therefore, the third principal stress is the most important stress in this thesis.

2.3.4 Von Mises stress

The von Mises stress is a scalar which is a combination of stress components. The definition is shown in equation 2.4 and uses the components of the Cauchy stress tensor. This stress gives a simple overview where stress concentrations occur and if they are close to the limits. However the individual components or other stresses must be evaluated when trying to understand the stress concentrations in more detail.

$$\sigma_v = \sqrt{\frac{1}{2}\left[(\sigma_{11}-\sigma_{22})^2 + (\sigma_{22}-\sigma_{33})^2 + (\sigma_{33}-\sigma_{11})^2\right] + 3\left(\sigma_{12}^2 + \sigma_{23}^2 + \sigma_{31}^2\right)} \tag{2.4}$$

2.4 DI-BSCCO types

SUMITOMO is the only producer of BSCCO tapes now. There are different tapes which meet different requirements, so depending on the needs of the application the proper tape can be selected.

Type H is the standard tape, where the H stands for High current density. So, this tape has no further reinforcements to it.

Type HT-SS is the standard type H with a stainless-steel reinforcement layer on both sides of the tape. The reinforcement is mainly there to increase the tensile strength of the tape. The stainless-steel doubles the critical axial tensile stress, while the thickness is only increased with 26%.

Type HT-CA is the standard tape which is reinforced with a copper alloy. This is used when a low splice resistivity is desired.

Type HT-NX has a similar goal as the HT-SS type, only the nickel alloy used in this type results in a much higher critical axial tensile stress than its stainless-steel counterpart.

Type G uses silver gold as matrix to reduce thermal conduction. This type is created to be used as current leads.

All these tapes have different applications, so is the 20 µm stainless-steel tape suitable for high-field large magnets and rotating machines in which a large electromagnetic force is applied to the conductor [17]. Whilst other tapes, such as 50 µm thick heat-resistant copper alloy tapes are good for power cables applications [17].

The tapes also handle industrial applications very well. SUMITOMO's DI-BSCCO tapes have been used in a pod propulsion system for ships, which is a very harsh environment to be operating in. Recently a 3 MW HTS ship motor [26, 27] has been made, which shows that the DI-BSCCO line from SUMITOMO is mature enough for high power applications.

2.5 DI-BSCCO Manufacturing

BSCCO tapes are manufactured according to the oxide-powder-in-tube method (OPIT) [28], where BSCCO filaments inside a silver matrix are constructed. At first the BSCCO powder is filled inside a tube, which is then isostatic compressed. It is done under isostatic compression to ensure the most uniform compression of the powder as possible. This compressed powder is then encapsulated inside a silver tube, which will become part of the silver matrix. The filament is then applied to a drawing process to reduce its radial dimensions. The desired number of filaments are then packed encapsulated in silver and drawn to reduce the multifilament wire to the wanted dimensions. This multifilament wire is then squeezed by rollers to make a flat tape. The final step for a non-reinforced tape is to apply a heat treatment, which converts to powder into the desired superconducting material. This process is shown in figure 2.3. Something that is not shown in the image is the controlled over pressure sintering [5], which takes place at the isostatic compression step. This step is crucial to increase the mechanical strength of the BSCCO tape. For reinforced tapes the final step is to apply the reinforced layer. Which is soldered onto the BSCCO tape. Depending on the requirements of the application different types of reinforced material can be used as described in section 2.4.

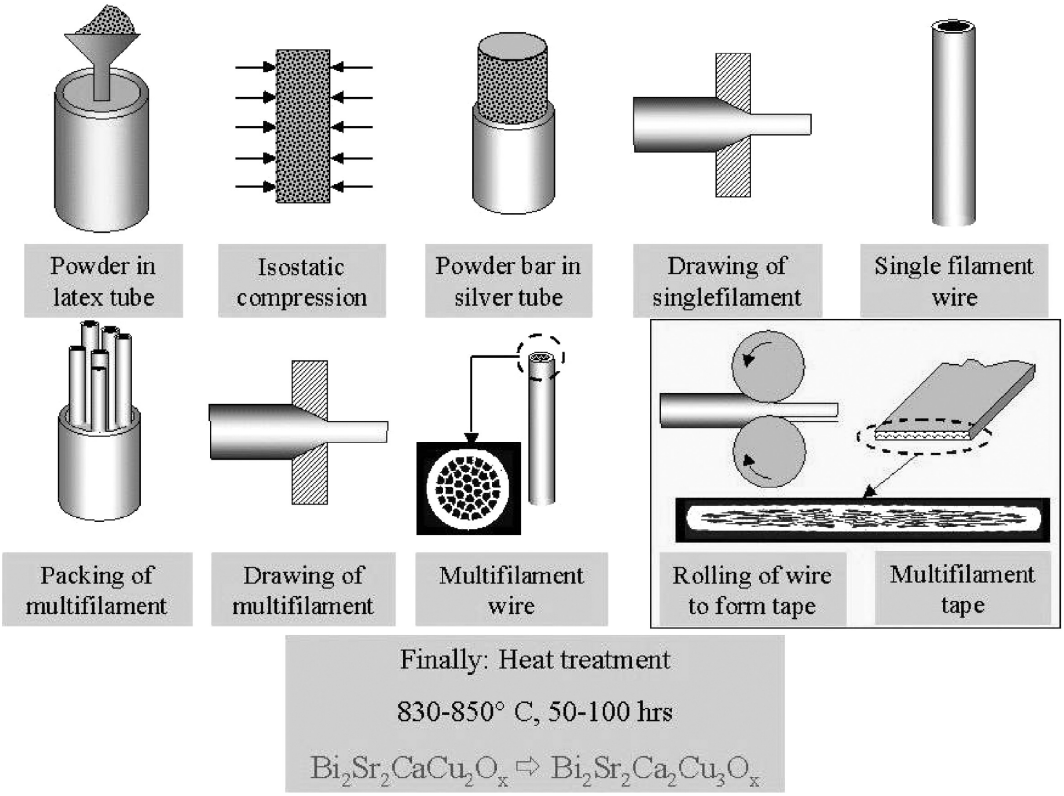

Figure 2.3: Overview of the OPIT process of BSCCO. [28]

3 | Experiments

3.1 Set-up

The entire measurement set-up consists of several parts and they can be split into two groups concerning the insert and the instruments. The insert will perform the cryogenic and mechanical side of the experiment, whilst the instruments will collect the data.

3.1.1 Insert

To see what transverse loads the tape is able to handle, a press is used. This press is specifically designed for measurements like these. The way it works is that the tape is squeezed between an anvil and a pushing head. This will deform the superconductor and as a result the critical current will reduce.

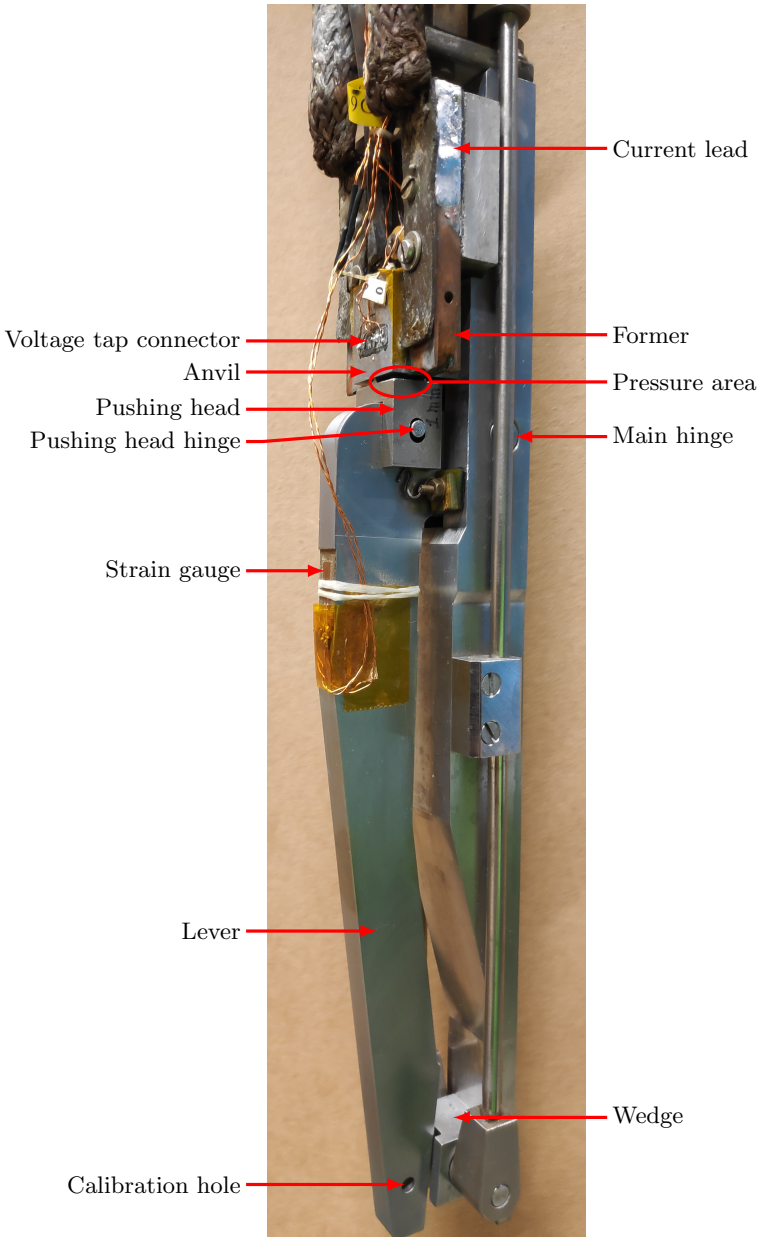

Figure 3.1: Insert for the transverse load measurements.

The press, which is used to do these transverse load measurements is shown in figure 3.1. The superconducting tapes are mounted along the former. The former consists of 2 copper pieces and a stainless-steel anvil. The copper pieces are also the current leads, to which the superconductor is soldered. The stainless-steel anvil is there to take the load of the press. To ensure that all the current will flow through the superconductor, Kapton® is placed between the current leads and the anvil.

The tape will be pressed between the anvil and the pushing head. The pushing head is a demountable part to be able to measure with different pushing head widths. A lever is used to get a mechanical advantage, which is needed to reach the range of operation stress levels. However only a lever is not enough to gain the necessary advantage needed to operate it by hand. A threaded rod runs from the top to the bottom of the insert. This rod can be rotated on the warm side using a knob. It will retract the small rods which are attached to

the wedge. This means that the wedge will exert a force on the lever when the knob on the warm end is turned.

To measure the exerted force a strain gauge is used, which is located on the outside of the lever. This means that when a force is exerted on the lever, the outside of the lever will compress, and the strain gauge is able to measure this. The strain gauge cannot be converted into a stress or force, without a calibration.

The calibration is done by applying a known force on the calibration hole. By using the distances of the main hinge to the calibration hole and to the pushing head hinge, a ratio can be determined. With the ratio, the applied calibration force, and the strain gauge a relation between the strain gauge value and the exerted force on the pushing head can be deduced.

To measure the I_c the voltage is measured with 2 voltage pairs. One pair is measured close to the region where the pushing head is located and the other is placed at a larger distance. This is done to see if the deformation has an unwanted influence on the closest voltage pair. These voltage taps are then soldered to the voltage tap connectors located on the insert. From which they are wired leading to the measurement equipment.

3.1.2 Instruments

The measurement equipment used to conduct this experiment has been put in an overview in table 3.1.

Table 3.1: Equipment used for measurements.

Data type	**Instrument type**	**In combination with**
Current	HITEC MACC+ zero-flux	Keithley 2700 multimeter
Strain gauge	Keithley 2700 multimeter	
Temperature	PT 1000	Cryo Con 24C
Pressure	Vaisala Digital Barometer PTB330	
Voltage taps	Keithley 2182A nanovoltmeter	
	Keithley 1801 nanovolt pre-amp	Keithley 2001 multimeter

Since the boiling point of liquid nitrogen is dependent on the atmospheric pressure, the pressure in the lab has also been recorded. In the earlier measurements the temperature sensor was not hooked onto the computer for digital readout, but in later measurements it was. Both are recorded to check if the behavior of I_c is due to applied force or to change in temperature.

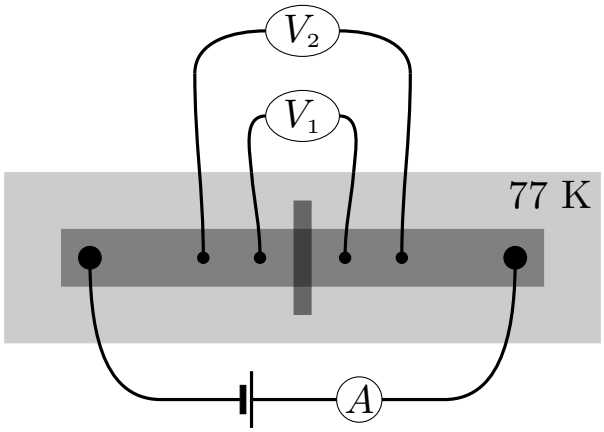

Figure 3.2: Circuit for measuring the IV-curves.

In figure 3.2 the electronic circuit is shown. There are two voltage pairs, which are each measured with two devices. Both voltage taps are measured using a Keithley 2182A nanovoltmeter. They are also measured at the same time using a Keithley 1801 nanovolt pre-amp in combination with a Keithley 2001 multimeter for readout. In the earlier measurements, just the nanovoltmeters were used. When the pre-amps became available, those were used as well. After analyzing some of the data, it was determined that only the pre-amps would suffice. The advantage of pre-amps is that the signal takes less time to become stable for readout, hence they are preferred. The circuit also shows which part of the circuit is submersed into liquid nitrogen and where the voltage pairs split to go to the different measurement devices. The middle-highlighted area over the superconductor is the pressure area. This is where the pushing head is pressing on the BSCCO tape.

3.1.3 Calibration

To be able to relate the measured strain on the strain gauge to the applied pressure, the setup has to be calibrated. First the strain gauge is done by applying a force on the calibration hole (see figure 3.1), perpendicular to the insert.

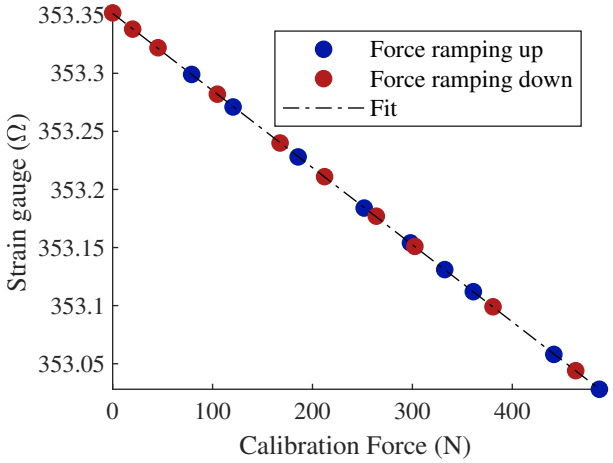

Figure 3.3: Strain gauge calibration.

In figure 3.3 the measured force is plotted against the resistance of the strain gauge at 77 K. This shows that the strain gauge behaves in the same way, whether the force ramping down or ramping up. The data has been fitted and the slope of the fit is shown in equation 3.1.

In figure 3.3 the resistance of the strain gauge at 77 K is plot against the measured force. This shows that the strain gauge behaves in the same way, whether the force ramping down or ramping up. The data has been fitted and the fit is shown in equation 3.1.

$$\text{Strain gauge calibration} = -6.6363 \cdot 10^{-4}\,\Omega\text{N}^{-1} + 353.3515\,\Omega \tag{3.1}$$

The calibration was also conducted in 2013 and the same relation was found, however it had a different offset. This means that the first term in equation 3.1 is important and the zero-strain value can be determined at the start of each measurement.

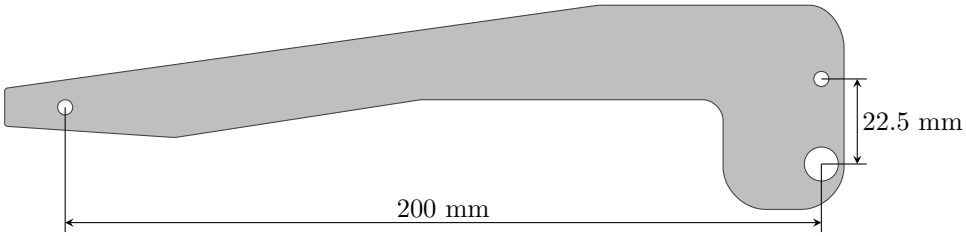

Figure 3.4: Schematic of the lever.

To relate the strain gauge to the actual force on the pushing head the mechanical advantage has to be taken into account. The ratio between the actual force and the calibration is the same as the ratio of the arms on which the forces are acting, with the main hinge as point of rotation. The lever and the lengths on which the forces act perpendicular are shown in figure 3.4. The ratio is as in equation 3.2.

$$\text{Force ratio} = \frac{200}{22.5} \approx 8.9 \tag{3.2}$$

3.2 Measurements

In short, the critical current is being measured as a function of stress. This will provide a degradation curve and a value for which permanent degradation begins to occur.

The details of mounting the sample and measurement procedure will be discussed in section 3.2.1 and 3.2.2 respectively.

3.2.1 Sample mounting

The tape is delivered on spool and need to be cut to the correct length. The length needs to be 18 to 19 cm, the way it is cut is not very important, since there will be plenty of contact area for current entry.

Next the voltage taps have to be soldered to the tape. When soldering, the temperature and the duration of the soldering have to be kept to a minimum. When the temperature gets too high, the composition of the superconducting material will change and therefore its superconducting properties. If the temperature is higher this process will speed up. Therefore, the aim is to keep the soldering time and temperature to a minimum. According to the manufacturer [29], the temperature should be maintained below 150 °C when soldering or heat treated for an extended period of time.

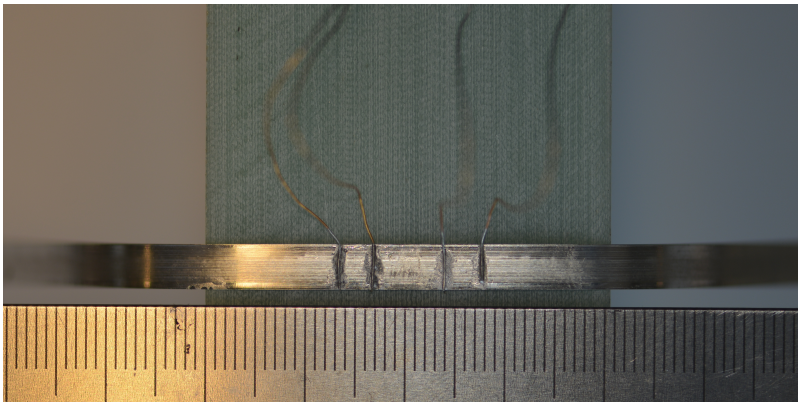

Figure 3.5: Voltage taps soldered to the superconducting tape. (Photo taken after measurement.)

The tape has a good heat transfer coefficient, which means that it will act as a heat sink when trying to solder. Therefore the method which works best is to heat the entire tape to an elevated temperature when trying to solder. The manufacturer [29] recommends $In_{52}Sn_{48}$ solder with SMD291 flux. This solder has a melting point of 119 °C. The sample has to be pre-soldered at the contact area of the current leads. First approximately 3.5 cm at the ends of the tape is pre-soldered, this is only done on one side of the tape, but for both current leads. Then the tape is flipped, and pre-solder is applied for the voltage taps. The voltage taps are then soldered into place, with as little solder as possible, as can be seen in figure 3.5. The entire tape is being kept at an elevated temperature of 110 °C, by an adjustable heating plate. The soldering iron is set to (its minimum temperature of) 150 °C. A small tip is used in the soldering iron when soldering the voltage taps.

The pushing head then needs to be installed on the insert. The way to do this is to remove the pin of the pushing head hinge, swap the pushing head for the desired one and push the pin back into place. The next thing to do is to slide the tape between the pushing head and the anvil, with the voltage taps sticking out. Carefully bend the tape around the former to the current lead. Solder the tape to the current leads, by first melting the solder on the current lead and then pressing the pre-soldered tape to the current lead. Then the voltage taps can be soldered to the wires that run along the insert top to instruments. They are soldered onto a copper plate to which both wires are soldered simultaneously.

3.2.2 Measurement Procedure

Before the measurements, the insert has to be inserted into the cryostat and the cryostat has to be filled with liquid nitrogen. When putting the insert into the cryostat, care should be taken to prevent damaging the strain gauge which is mounted on the lever. Then the cryostat has to be filled, the level should be above the minimum level, which can be checked by a change in voltage over an LED. The voltage drops when the led is submersed into the liquid nitrogen. As mentioned in appendix A care should be taken when handling liquid nitrogen.

When the sample and insert have been cooled down, the actual measurements can begin. First a baseline measurement is taken at 0 MPa. This will result in the critical current before any stress is applied. After the baseline, the stress is increased step by step. After each increment, the critical current is measured at that applied stress level and also after releasing the stress back to 0 MPa. This way the irreversibility limit can be found.

Each individual measurement consists of a measured IV-curve, of which the critical current is determined. The data points for the IV-curve are taken with a set loop. First the current is ramped to the desired current, after which a pause is taken to filter out any noise on the signal, before the measurement is taken. This is called the settle time. This lays in the order of a couple of seconds. Between the readout of each instrument half a second is taken to prevent any noise. After this is done, next ramp in current will take place. This happens until the electric field of the inner taps exceeds 10 times the critical electric current.

The measurements of the IV-curves are fully automated and the data is saved to a file. The change in applied tape pressure has to be done manually. From the multimeter of the strain gauge, the actual pressure can be deduced and therefore can be used to set the correct pressure. When overshooting the target pressure, it is not possible to go back to a lower pressure, since irreversibility has to be taken into account.

4 | Model

4.1 Tape properties

4.1.1 Material properties

For the FEM analysis some material properties are required. These properties are shown in table 4.1. The simplified area in the simulations containing BSCCO and silver have combined properties which are deduced in section 4.1.2 with the rule of mixtures.

The Kapton® insulation which is used around the BSCCO as well as the impregnation epoxy are not specified by the manufacturer. Therefore, some assumptions have been made about the material properties. Most Kapton® products have similar properties, so Kapton® HN is used for its material properties since this product is suitable for cryogenic temperatures.

The epoxy which has been chosen as reference material is CTD-101K, because this is a commonly used epoxy in superconducting coils [30]. Its mechanical properties are well documented and therefore it is suitable for the simulations.

Table 4.1: Material properties.

E is the Young's modulus, ν is the Poisson's ratio, ρ is the Density, σ_y is the initial yield stress, E_t is the Isotropic tangent modulus and μ is the friction coefficient.

Material	Part	E [GPa]	ν	ρ [kg/m^3]	σ_y [MPa]	E_t [GPa]	μ	Comments
SS 316	PH, Anvil	209	0.283	7970	–	–	–	[12]
SS 304	SS layers	214	0.278	7860	1400	95.8	0.3	[12, 31, 32]
Ag	Matrix	89.1	0.362	10618	56.6	0.351	–	[2, 33]
BSCCO	Filaments	127.0	0.14	6000	–	–	–	[34]
BSCCO/Ag	Filaments & Matrix	110	0.237	8023	56.6	50.2	–	Rule of mixtures with a BSCCO fill factor of 56%.
Kapton®	Insulation	2.76	0.34	1420	–	–	–	[35]
Epoxy	Filler	16.7	0.34	1030	–	–	–	[36, 37] CTD-101K

4.1.2 Rule of mixtures

The properties of a composite material can be estimated by taking the weighted average of the materials [38]. This weight is based on the volume of the material. In this case a fill factor f of 56% BSCCO is used. The combined properties of BSCCO/Ag are determined using equations 4.1.

$$E_{BSCCO/Ag} = fE_{BSCCO} + (1-f)E_{Ag} \tag{4.1a}$$
$$\nu_{BSCCO/Ag} = f\nu_{BSCCO} + (1-f)\nu_{Ag} \tag{4.1b}$$
$$\rho_{BSCCO/Ag} = f\rho_{BSCCO} + (1-f)\rho_{Ag} \tag{4.1c}$$
$$\sigma_{y\,BSCCO/Ag} = \sigma_{y\,Ag} \tag{4.1d}$$
$$E_{t\,BSCCO/Ag} = fE_{BSCCO} + (1-f)E_{t\,Ag} \tag{4.1e}$$

The young's modulus $E_{BSCCO/Ag}$ holds for the elastic regime, which ends when Ag reaches its yield stress. After that the isotropic tangent modules determines the shape of the stress strain curve. $E_{t\,BSCCO/Ag}$ consists of the young's modules of BSCCO and the isotropic tangent modules of silver, because the silver matrix experiences plastic deformation and the BSCCO is still in the elastic regime. The density and Poisson's ratio are independent of the regime.

4.1.3 Image tracing

To get an accurate simulation, it is best to simulate the geometry of the tape as close to reality as possible. In order to do so, a photo of the cross section has been made. This photo can be seen in figure 4.1a.

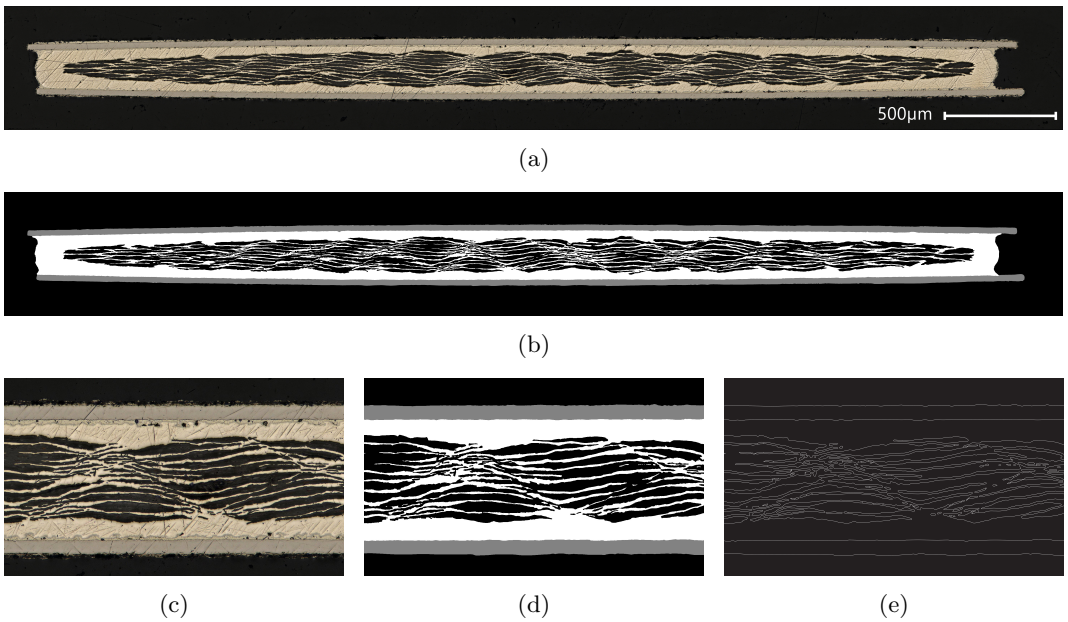

(a) (b) (c) (d) (e)

Figure 4.1: Polished cross section of BSCCO-2223 stainless-steel reinforced tape. (a) High resolution photo taken with a microscope. (b) Image processed with editing software to separate materials using into different shades of gray. (c, d, e) Zoomed in on a part of the cross section, with the photo, edited photo and vectorized contour respectively.

The image processing result can be seen in figure 4.1. The first step in the process is to get rid of the scratches, which are left from the polishing process. Then the silver matrix, BSCCO filaments and the stainless-steel reinforcement layers are given their own shade of gray. The result of this can be seen in 4.1b. The last step is to convert the gray scale image to a vectorized contour file, which can be used as geometry input by COMSOL. A comparison of the same part of the photo is shown in figures 4.1c,d,e.

4.2 Model of the experimental setup

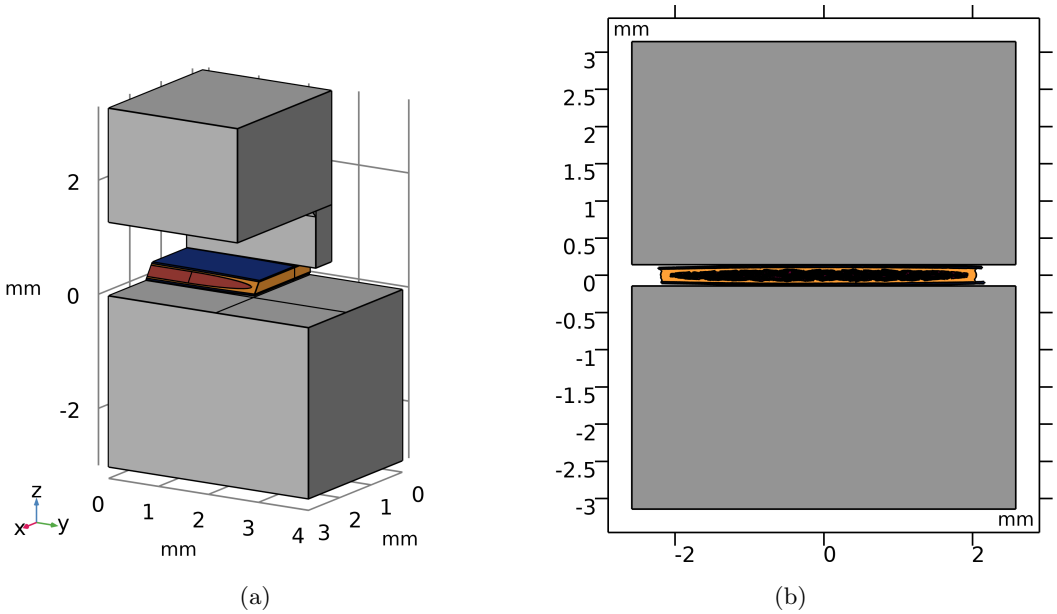

(a) (b)

Figure 4.2: Geometry of the simulated experiment. (a) 3D model. (b) 2D model.

The experiment described in chapter 3 is simulated using COMSOL. In figure 4.2 an overview of the 2D and 3D geometries are shown, these simulations are explained in detail in sections 4.2.1 and 4.2.2 respectively.

The main reason for the 3D simulation is the 3D edge effect which come into play when pressing on a tape. This means that the stresses are not uniform in the x-direction of the 3D model. The caveat is that the image traced tape cannot be used, due to its increased computation time. Therefore, a simplification has been made, which is to approximate the BSCCO filaments as a uniform single piece with the material properties deduced in section 4.1.2. To validate the approximation a 2D comparison is made and the 2D geometry is also used to gain an insight of the significance of the 3D effects.

The degradation is quantified, by a third principal stress criterion. It is assumed that the BSCCO filaments perform without degradation until failure. The COMSOL models simulate the principal stresses as a function of applied transverse pressure. Which connects the experimental data to the simulations.

4.2.1 2D Models

The goal is to simulate the principal stresses as a function of applied (experimental) pressure. Figure 4.2b shows the geometry of the 2D simulation. The model contains 3 separate objects. BSCCO superconducting tape sandwiched by 2 blocks of steel at the top and bottom. The material properties and its color codes are shown in table 4.1. The model is purely mechanical, and the pressure is applied via a displacement.

The bottom boundary of the anvil is fixed, and the top boundary of the pushing head is displaced through the means of a parametric sweep. There are two contact pairs defined. The first one is between the lower boundary of the pushing head and the upper boundary of the top stainless-steel reinforcement layer. The second is between the top boundary of the anvil and the lower boundary of the bottom stainless-steel reinforcement layer. This way COMSOL will dynamically adjust the contact region and pressure according to the set displacement.

For stability a body force and a friction force are introduced. When the pushing head meets the tape, the tape is pushed away, and this creates an instability. To counter this a weak spring force is applied to the tape, which results in the tape pushing back into the pushing head. This weak spring force is brought to zero when the tape also meets the anvil. Another point of instability is also reached at this moment. The tape is namely free to move from side to side and therefore the tape can move out from in between the pushing head and anvil. This is fixed by a friction force in the contact pairs. This force keeps the tape from moving freely and therefore the simulation becomes stable.

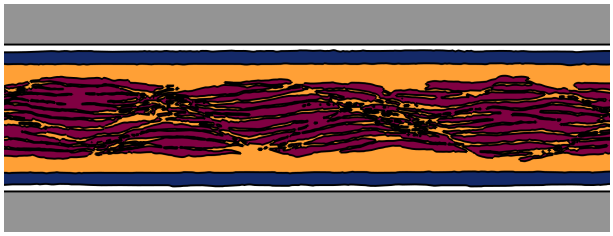

Figure 4.3: Zoomed in section of the 2D image traced tape geometry.

Shown in figure 4.3 is the geometry which is the result of the image tracing described in section 4.1.3. The filaments are clearly visible, and the surface of the reinforcement layer is a bit rough. This is the first step of the 2D simulations which will be conducted.

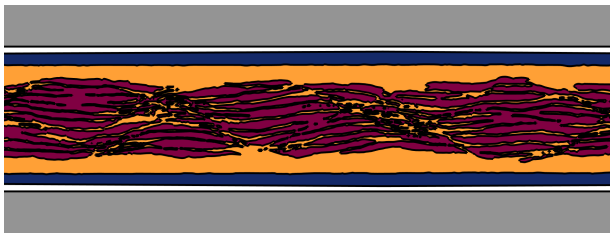

Figure 4.4: Zoomed in section of the 2D image traced tape geometry with smoothed reinforcement layer.

There are two reasons why the surface from the reinforcement layer is not smooth. The first one is the effect of smearing of softer material during the polishing and the second one is due to the image processing. The reason for the second one is the vectorization of the image. The stainless-steel layer gets a unified gray tint and to preserve as much of the BSCCO filaments geometry as possible, the vectors follow the pixels quite well.

Both effects result in the fact that the surfaces are no longer smooth, which is negligible for the shape of the filaments, silver matrix or inside of the stainless-steel layer. However, for the contact boundary it creates pressure points during the mechanical simulation. Therefore, the contact boundary is smoothed. This can be seen in figure 4.4.

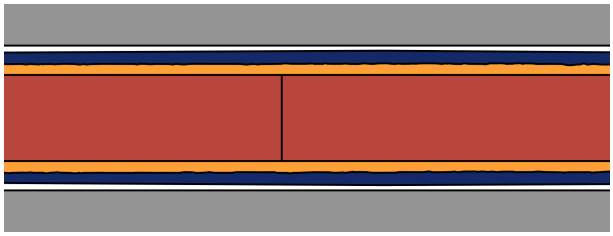

Figure 4.5: Zoomed in section of the 2D simplified rule of mixtures geometry.

To validate the use of the rule of mixtures in the 3D simulation, a comparison is made in 2D. The imaged traced tape model with smoothed reinforcement layer is used, with the only difference being that the filaments are not separately existing anymore. The filaments have been replaced with a geometry of BSCCO/Ag with properties derived with the rule of mixtures, see section 4.1.2. A zoomed in section of this model is shown in figure 4.5. The replaced BSCCO/Ag geometry is the same as the 3D case. This way a check can be performed, whether the third principal stress as failure criterion produces the same failure rate in both the filaments and rule of mixtures case.

4.2.2 3D Model

The 3D simulation does the same as the 2D simulations described in section 4.2.1. There are a few key differences between the 3D and 2D simulations. The obvious one is that the 3D geometry contains a non uniform 3rd dimension. The model has 2-fold symmetry and therefore only a quarter has to be simulated. An overview of this has been shown in figure 4.2a. The boundaries which are attached to the xz- and yz-planes have the symmetry property. As a side effect the model becomes more stable, since nothing can move away. This means that the friction did not need to be applied on the contact surfaces. It was not necessary to include a weak spring in the 3D case, to get the system stable. The contact fixed and displaced boundaries in the 3D simulation are the same as the 2D simulation.

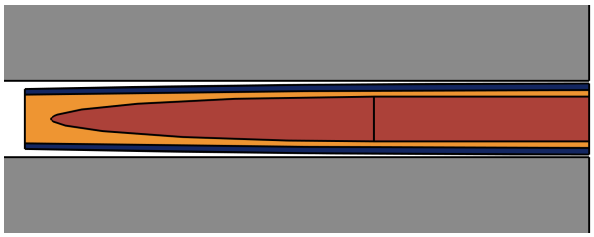

Figure 4.6: Simplified geometry of the tape in the 3D model, displayed in the yz-plane.

In order to decrease the number of points in the mesh the entire geometry of the tape has been simplified. As can be seen in figure 4.6 the stainless-steel reinforcement layers of the tape are not parallel to the anvil and pushing head. The curvature can be approximated with an ellipse. The overhang of the reinforcement layers is not important for the simulations, so the sides are straight to decrease the degrees of freedom in the model. A zoomed section of the tape in the yz-plane can be seen in figure 4.6.

4.3 Single tape inside Flutter coil

Varian's Flutter coil consists of 6 double pancakes, with 786.5 turns in total. Since all the tapes inside the coil are the same, only a single tape is modeled for the worst case condition. The failure of the tape can be deducted from the failure criterion of the BSCCO filaments, which is deduced from the 3D model and the experiments. The transverse load at which this tape is expected to fail is then compared to highest transverse compressive stress inside the coil, to determine the mechanical stability margin of the coil.

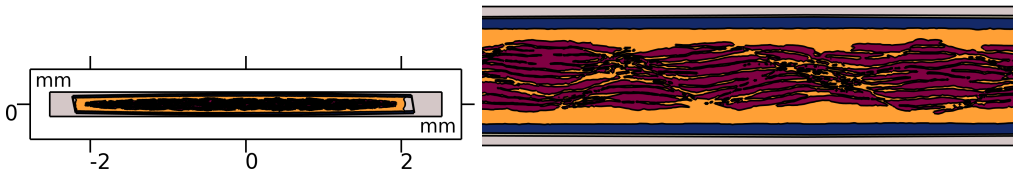

(a) (b)

Figure 4.7: Geometry of a single tape inside the Flutter coil. (a) Overview of the entire geometry. (b) Detail up of the tape cross section geometry.

Since this single tape is part of a stack in the coil, symmetry for the boundary conditions is assumed. The tapes in the winding pack are also individually insulated with a 5 µm thick Kapton® layer and the remaining space is filled up with epoxy. The top of this epoxy part is displaced in the model and the bottom boundary is fixed.

5 | Results and discussion

5.1 Experimental results

5.1.1 Samples

A total of 10 samples of the Sumitomo tape have been measured. An overview of these tapes samples is shown in table 5.1.

Table 5.1: Sample data properties.

Sample name	**Pushing head**	**Inner V-tap (mm)**	**Outer V-tap (mm)**	**Solder**	**Soldering temperature (°C)**	**Measuring instrument**	**Comments**
SUMI#1	1 mm	11.34	26.12	$Sn_{62}Pb_{36}Ag_2$	230	Nano	Measured without taking the pressure off the sample.
SUMI#2	1 mm	11.2	31.3	$Sn_{62}Pb_{36}Ag_2$	230	Nano	
SUMI#3	1 mm	11.2	31.3	$Sn_{62}Pb_{36}Ag_2$	220	Nano	Failed measurement: Pushing head partly in contact with solder of voltage taps.
SUMI#4	1 mm	8.0	29.8	$In_{52}Sn_{48}$	150	Nano	Failed measurement: Pushing head partly in contact with solder of voltage taps.
SUMI#5	1 mm	4.2	10.2	$In_{52}Sn_{48}$	150	Nano	
SUMI#6	1 mm	4.8	11.1	$In_{52}Sn_{48}$	150	Nano	
SUMI#7	4 mm	6.5	10.3	$In_{52}Sn_{48}$	150	Nano & PreAmp	Used for settle time tests.
SUMI#8	2 mm	3.7	11.4	$In_{52}Sn_{48}$	150	Nano & PreAmp	Failed measurement: Pushing head partly in contact with solder of voltage taps.
SUMI#9	2 mm	7.0	–	$In_{52}Sn_{48}$	150	PreAmp	Both PreAmps connected to same voltage pair.
SUMI#10a	2 mm	7.2	14.4	$In_{52}Sn_{48}$	150	PreAmp	
SUMI#10b	1 mm	7.2	14.4	$In_{52}Sn_{48}$	150	PreAmp	Remeasured sample SUMI#10a, with 1 mm pushing head.

Some measurements were not considered eligible when drawing conclusions. SUMI#1 has been measured without returning to zero force after each step. Therefore no conclusions can be drawn for the irreversibility criterion. SUMI#3 and SUMI#4 had too much solder on one of the voltage taps, which caused contact between solder and pushing head during the experiment. As can be seen in figure 5.1ab, as a result the pressure was not homogeneously distributed and no meaningful conclusion could be drawn. This issue has been solved for every consecutive measurement starting with SUMI#5. The pushing head has been milled to have more clearance without changing the width of the contact area. The gap between the solder of the inner voltage pair of SUMI#8 is too small. This causes a small bit of solder to be trapped between the pressure area of the pushing head and the tape. As can be seen in figure 5.1c.

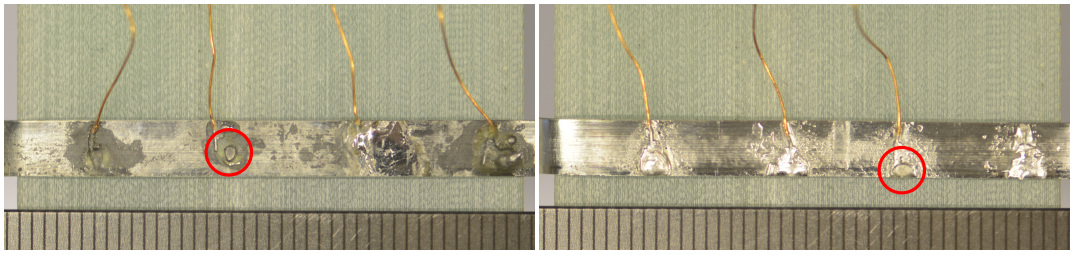

(a) (b)

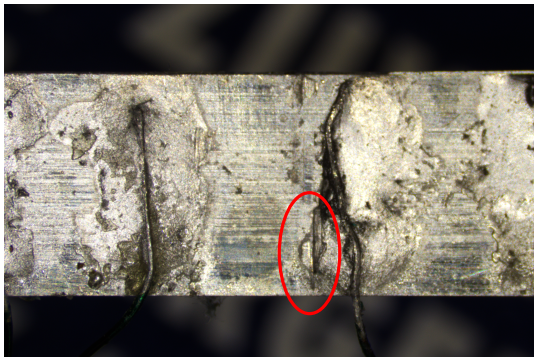

(c)

Figure 5.1: Solder in contact with the pushing head during the experiment. (a) SUMI#3. (b) SUMI#4. (c) SUMI#8.

5.1.2 Pushing head of 1 mm

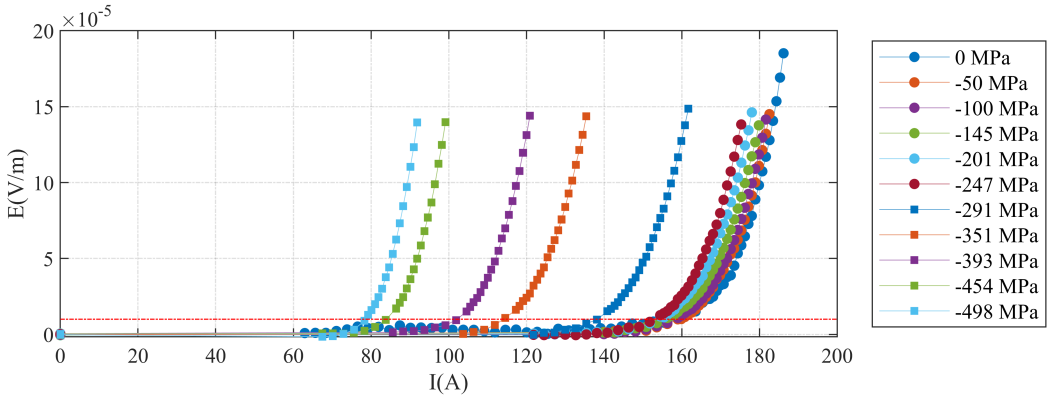

Figure 5.2: SUMI#6, 11.1 mm voltage pair. Electric field as a function of current for several pressures.

In figure 5.2 the $E(I)$-curves are shown for the 11.1 mm voltage pair of SUMI#6. The $E(I)$-curves look clean with no unexplainable data points or errors. Therefore, the I_c points obtained from these curves are considered valid. The same can be said for the other samples and voltage pairs.

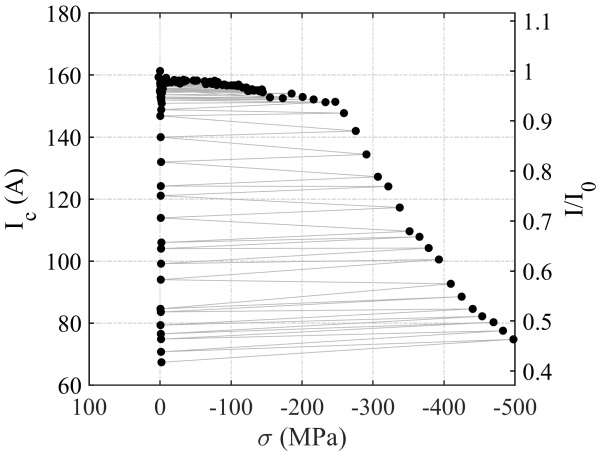

Figure 5.3: SUMI#6, 11.1 mm voltage pair. I_c as a function of the experimental stress.

The irreversibility is determined by going back to zero force after each increment in applied transverse pressure. For SUMI#6 this is shown in figure 5.3, where the light gray lines show the sequence of measurements.

The irreversible I_c as a function of experimental stress is constructed by taking the I_c at zero force and the highest stress it has experienced prior to this measurement. The 1 mm pushing head experiments all follow roughly the same shape, as can be seen in figure 5.4. This shows that SUMI#2, SUMI#5 and SUMI#6 are in agreement. They all degrade irreversibly around $\sigma = -250\,\text{MPa}$, with roughly the same rate.

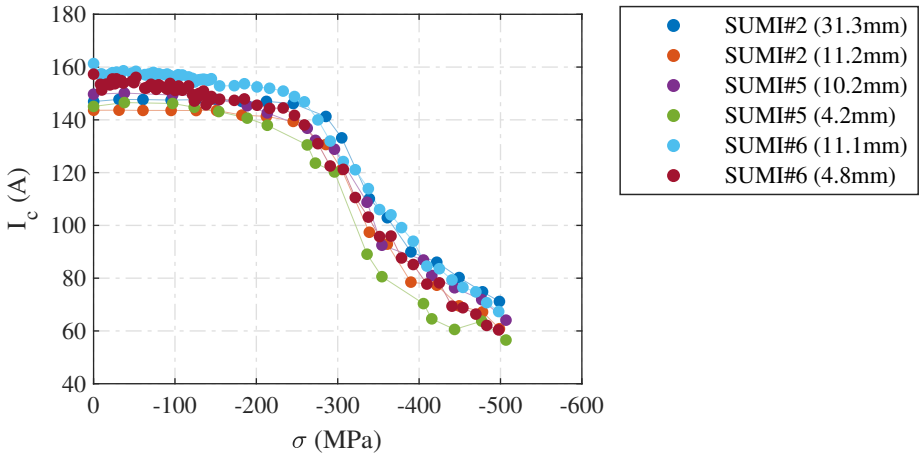

Figure 5.4: Irreversible I_c as function of the experimental stress.

The voltage pairs with a larger distance between them show a higher I_c than the voltage pairs with the smaller distance on the same tape. This is because when the degradation begins the voltage over the damaged area increases. However, the voltage taps are placed somewhat further away from that region, so when dividing by the distance of the voltage pair, the average electric field of the wider voltage tap is lower. This then results in a somewhat higher I_c at the same E_c criterion.

The atmospheric pressure, dictates the boiling point of the liquid nitrogen. Therefore, the actual testing temperature of the samples deviates slightly and causes a spread in the I_c. The homogeneity of the tape might not be perfect as well and some minor differences are therefore expected.

5.1.3 Pushing head of 2 & 4 mm

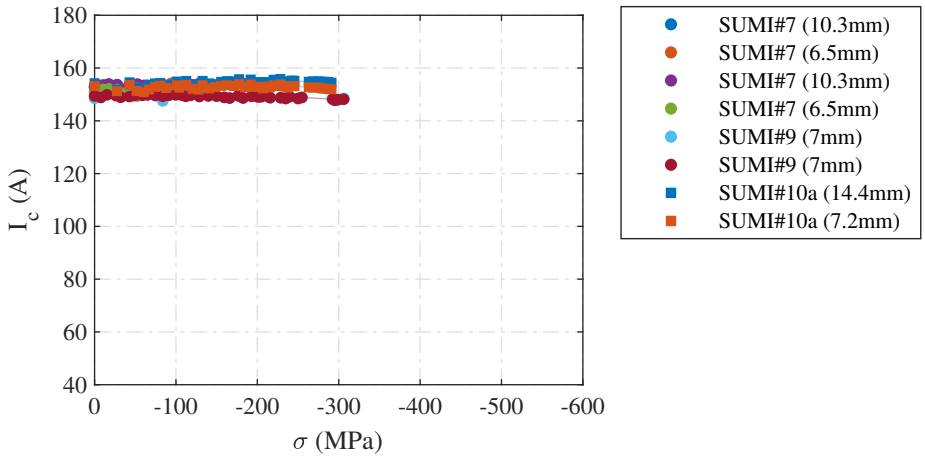

Figure 5.5: Irreversible I_c as function of the experimental stress.

The experiment on SUMI#7, which is the only sample on which a 4 mm pushing head was used, did not degrade in I_c, due to the limited stress of the setup. So, the only conclusion which can be drawn from the 4 mm experiment is that the tape does not degrade when the transverse compressive pressure does not exceed 125 MPa.

SUMI#9 and SUMI#10a, performed with a 2 mm pushing head, did not degrade up to the limits of the setup. Although speculative, it is suggested that this might be related to the dislocation of softer material occurring when the tape is compressed. Instead of only getting thinner under pressure, the softer material deforms plastically and this is pushed outwards from underneath the pushing head. This material finds resistance by the materials outside the pushing head region that are not compressed and is attached to the stainless-steel reinforcement layer and the harder materials like the superconducting filaments. When the pushing head becomes wider, more material has to be relocated over a larger distance to reach the same displaced at with a 1 mm pushing head. Less plastic deformation, i.e. less dislocation of the silver, means less deformation and less tensile strain on the filaments, and thus a higher transverse stress is allowed before irreversible degradation is reached. This is in contradiction with the results reported in reference [9], as presented in section 2.2.1.

5.1.4 SUMI#10

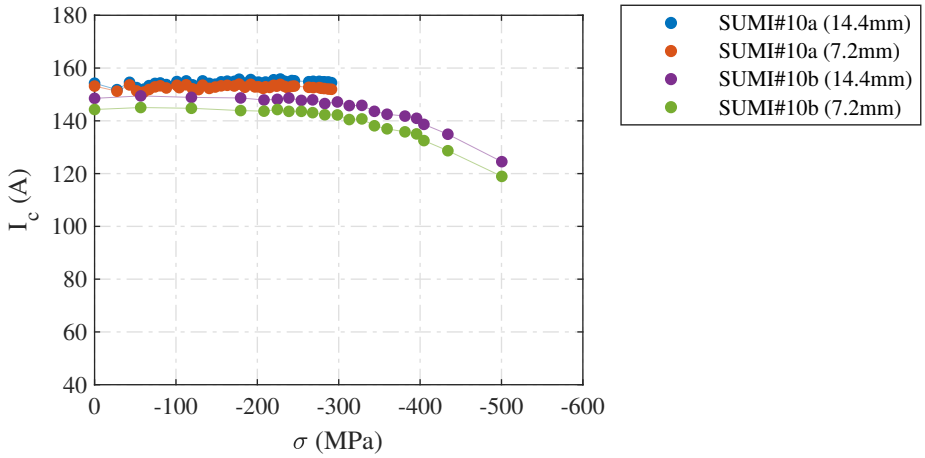

Figure 5.6: Irreversible I_c as function of the experimental stress.

After the 2 mm pushing head was used, the same sample was loaded with the 1 mm pushing head in order to find the effect on the I_c. The tape degraded at a higher pressure, compared, as the other 1 mm pushing head experiments. This might be due to the plastic deformation of the softer materials (silver), which is caused by the prior experiment, where the 2 mm pushing head was used.

It is suggested that this could be related to the fact that the tape is not perfectly flat, but has sort of an elliptical shape as can be seen in figure 5.10. The 2 mm pushing head deformed the tape in such a way that the thickness of the tape is reduced in the center. Therefore, to reach the same stress concentrations, the 1 mm pushing head has to be pushed down further.

The experimental stress is characterized by the width of the tape times the width of the pushing head. When subjected to a downward displacement of the pushing head the elliptical shape of the tape dictates the width of the contact area. The load is better distributed when the actual contact area increases and therefore it seems that the degradation of I_c takes place at a higher critical stress.

5.2 Model results

5.2.1 Model of the experimental setup

First, the results from the model, which simulates the experimental setup with tape, are shown. These results are going to give better insight into the experimental conditions, and this will then be used to draw conclusions for the Flutter coil further on in this thesis.

2D Models

The initial two tape models which are compared are the smoothed reinforcement layer model and the purely imaged traced tape. Both of these models are shown in figure 5.7. The difference between these two simulations is that the contact surface of the purely imaged traced one is rough and therefore creates pressure concentration points in the calculation results. Since this level of roughness is not realistic and increases the computation time, the smoothed model is used for the next simulations.

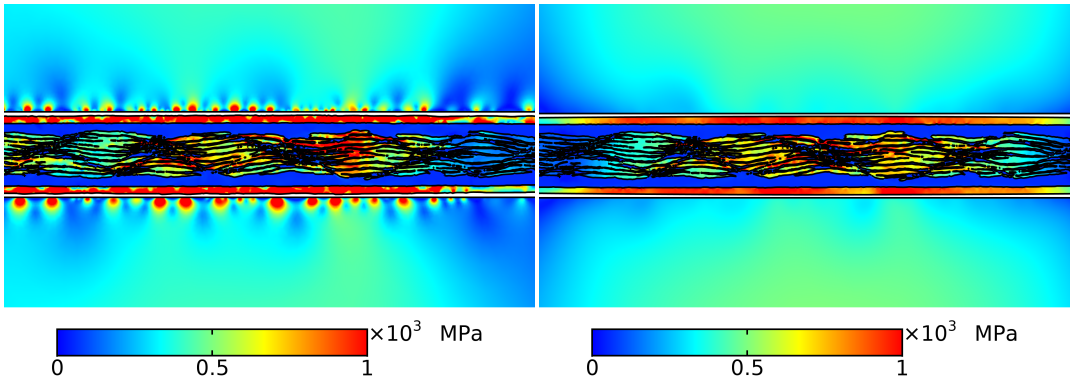

(a) (b)

Figure 5.7: Von Mises stress. (a) Imaged traced tape under an experimental pushing head pressure of −213 MPa. (b) Imaged traced tape with smoothed reinforcement layer under an experimental pushing head pressure of −214 MPa.

The 2D model with filaments and smoothed reinforcement layer is compared to a 2D model, which has its filaments replaced with a simplified geometry based on the rule of mixtures. A normalized surface area of the superconducting filaments, which have not failed (not exceeded the irreversibility limit) is compared with the normalized surface area which has the properties defined by the rule of mixtures. This comparison has been made at several failure criterion of which the −525 MPa and −775 MPa failure criteria examples are shown in figure 5.8.

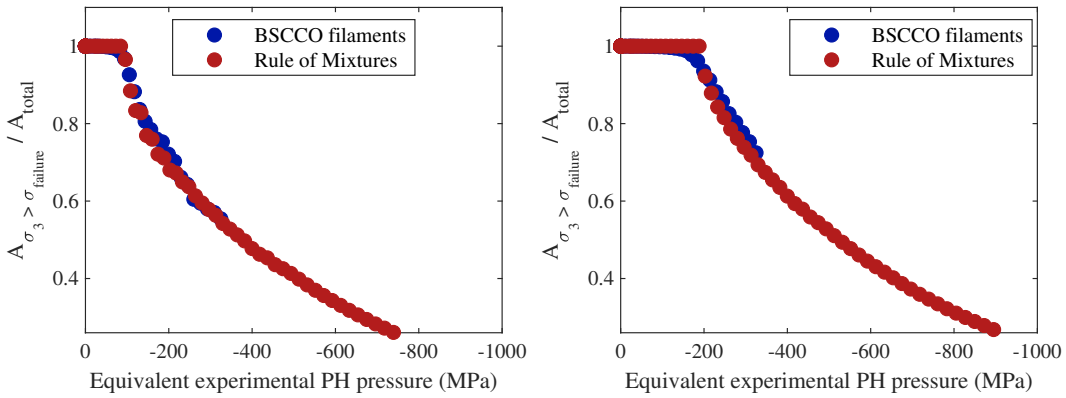

(a) (b)

Figure 5.8: Comparison between the 2D simulation with actual filaments and the simplified rule of mixtures geometry. (a) $\sigma_3 = -525$ MPa failure criterion. (b) $\sigma_3 = -775$ MPa failure criterion.

These comparisons show that the rule of mixtures model deviates with a maximum of 5% from the actual filaments model. This confirms that the rule of mixtures approximation yields a valid result when performing mechanical analysis on the tape. Due to the uniformity of the rule of mixtures approximation, the initial failure is quite sudden. Whereas the failure for the filaments progresses more gradually, due to the irregularities in the shapes of the BSCCO filaments. These variations in stress concentrations are shown in figure 5.9a. In figure 5.9b the rule of mixtures model is shown and there are no variations or stress concentrations present.

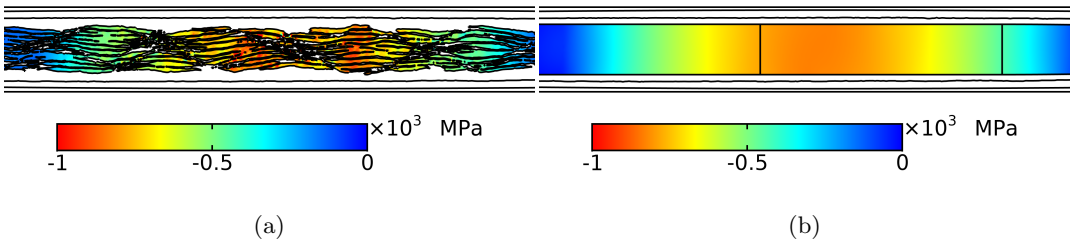

(a) (b)

Figure 5.9: Third principal stress inside the BSCCO filaments and the combined Ag/BSCCO material based on the rule of mixtures. (a) BSCCO filaments with the tape experiencing an equivalent experimental pushing head pressure of −214 MPa. (b) Ag/BSCCO with the tape experiencing an equivalent experimental pushing head pressure of −218 MPa.

3D Model

Stress concentrations and deformations caused by the edge of the pushing head can only be evaluated properly in a 3D model, with the volume shape of the tape taken into account. The deformation and stress in the original x-direction of the tape can be seen in figure 5.10. The colors correspond with a stress and the lines with a displacement in the x-direction, respectively. The gray lines correspond with the initial position of the tape in the x-direction and the solid black lines correspond with the displaced material after applying a load of $-245\,MPa$. Note that the black lines have a factor 2.5 on the displacement for better visibility.

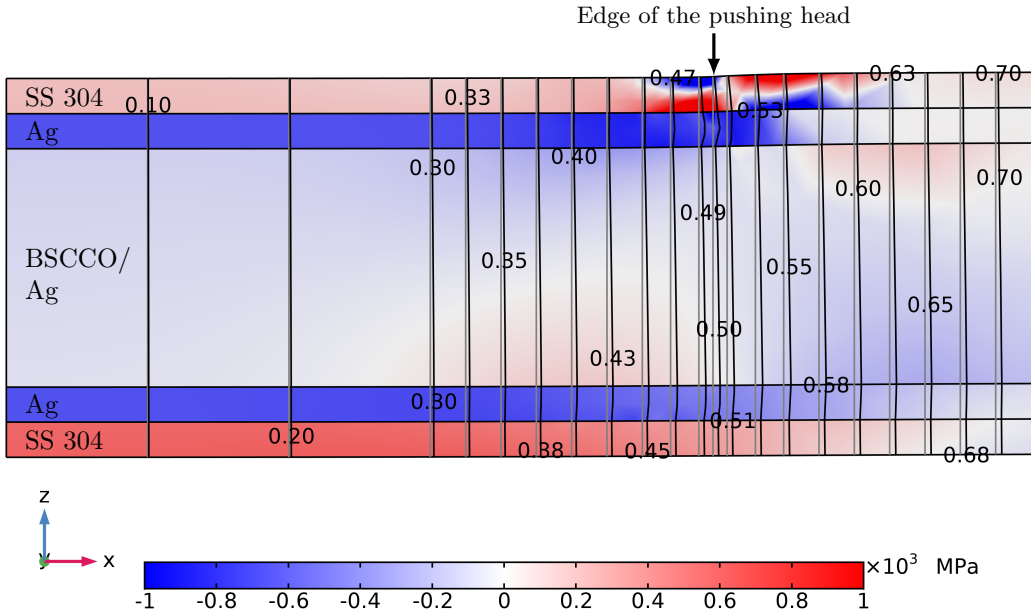

Figure 5.10: Second Piola-Kirchhoff stress and displacement lines in the x-direction, respectively. Under an equivalent experimental pushing head pressure of −245 MPa.

Figure 5.10 illustrates that the soft silver is under compressive stress. This means that the silver is plastically deformed and being squeezed out in planar plane direction by the force of the pushing head, creating tensile strain in x-direction. The same effect can be assumed in y-direction, which means tensile loading of the filaments until breakage. This

can also be seen by the displacement lines. The stainless-steel is under tensile stress, which means that the reinforcement layer is holding the tape together in compression.

At the edge of the pushing head, the stainless-steel layer distributes the mechanical load over the softer silver. This can be seen by the compressive and tensile stress concentrations at the edge of the pushing head. The stainless-steel is resisting the bending motion, which is happening at the edge and just past the edge. The pushing head is displacing the stainless-steel, but the tape is holding itself in shape where the pushing head is not applying transverse stress. This is causing a height difference and results in the S-bend. This also results in the net transverse stress in the top stainless-steel layer just outside the pushing head. Since the bottom stainless-steel layer is in contact with a flat surface, the tensile stress is less. The result of this is that the tape curls upward outside the pushing head, which is in turn causing the higher tensile stress in the middle of the bottom reinforcement layer.

To compare the simulation with the experiment, the correct cut plane has to be evaluated. The cut plane has been determined based on the results of the entire geometry, which is shown in figure 5.11a. A balance needs to be made when defining the cut plane.

It is desired to have the plane as perpendicular to the current as possible, to limit any effects of current redistribution. Since the BSCCO filaments extrude in the x-direction the plane may rotate a little bit over the y-axis and still hold a good result. It is also desired to have the cut plane in the maximum compressive third principal stress, since that is where the BSCCO will fail. Due to the 3D effect the stress concentration on the top of the BSCCO/Ag is higher than the bottom. This is caused by the asymmetry between the pushing head, which has a fixed width and the anvil, which is flat. With all of this taken into consideration the cut plane which is shown in figure 5.11b is expected to be the limiting plane in terms of failure.

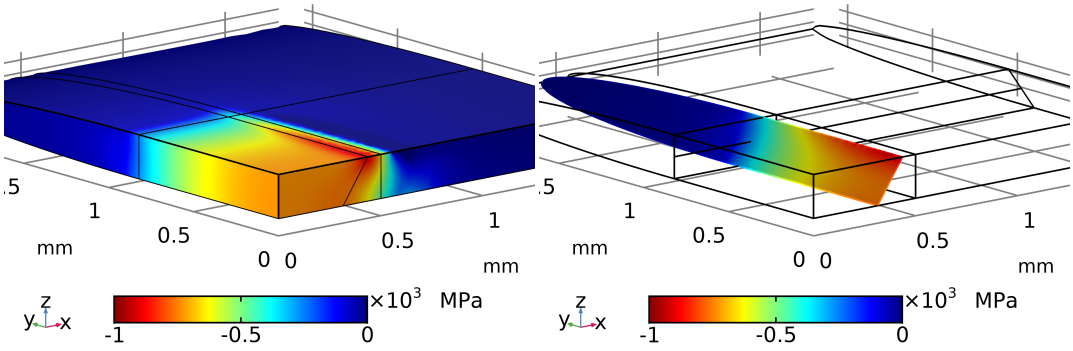

(a) (b)

Figure 5.11: Third principal stress inside the combined BSCCO/Ag material, whilst experiencing an equivalent experimental pushing head pressure of $-245\,\mathrm{MPa}$. (a) Entire BSCCO/Ag geometry. (b) Cut plane over which the failure criterion is evaluated.

The simulation returns a distribution of the third principal stress inside this defined cut plane, for all the simulated steps. These steps are linked to the equivalent experimental pushing head pressure. With the third principal stress distributions and pushing head pressures, the failure curve can be determined, given a failure criterion. Curves with different failure criterion were made and the one with the best fit to the measured data shown in figure 5.4, is presented in figure 5.12. This curve was constructed with a failure criterion of $\sigma_3 = -775\,\mathrm{MPa}$ and this is considered as the compressive pressure at which the BSCCO fails.

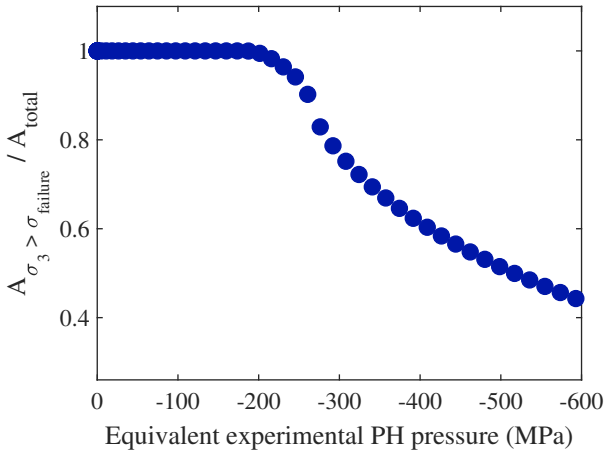

Figure 5.12: Failure of the critical part of the tape as a function of the equivalent experimental pushing head pressure, with a failure criterion of $\sigma_3 = -775\,\text{MPa}$.

A few areas can be defined when it comes to the degradation curve in figure 5.12. The first area up till $\sim -190\,\text{MPa}$, shows no degradation. The next area till $\sim -290\,\text{MPa}$ shows a progressive degradation. There is a small area at the top, close to the edge of the pushing head which reaches the failure criterion first. This then slowly expands across the width of the tape and downward. The last area is from $\sim -290\,\text{MPa}$ onward. In this area the height of the tape starts to be saturated with failed material and therefore the failure contour can only expand to the sides of the tape. But due to the curved shape of the tape it gets progressively harder to squeeze more of the side of the tape. This also explains why the results of the measurements shown in figure 5.4 have the same shape.

5.2.2 Single tape inside Flutter coil

The final simulation is that of a tape inside the Flutter coil. With the BSCCO filament failure criterion of $\sigma_3 = -775\,\text{MPa}$ which has been found through the match between experiment and the 3D model, a failure curve as function of transverse load can be made. This is shown in figure 5.13.

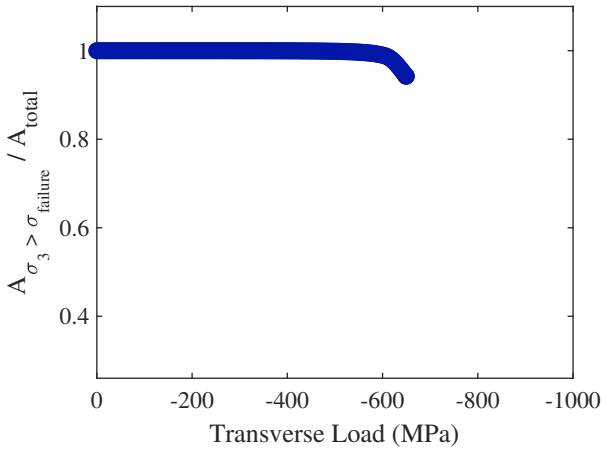

Figure 5.13: Failure of the coil as a function of transverse compressive stress, with a BSCCO filament failure criterion of $\sigma_3 = -775\,\text{MPa}$.

According to the simulations which have been conducted by ECO5, the coil experiences a maximum transverse load of $\sim -140\,\text{MPa}$ [39]. The simulation which has been conducted as part of this thesis shows that the 99% I_c-criterion is reached at $\sigma_{Transverse\,Load} = -600\,\text{MPa}$. This means that there is still a safety margin of approximately 300% when the coil is under full load.

Figure 5.14a shows the load which the coil reaches during operation and figure 5.14b shows the load at the point of degradation.

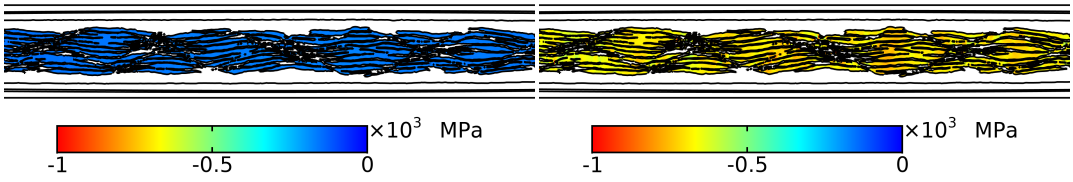

(a) (b)

Figure 5.14: Third principal stress inside the filaments of the coil. (a) Transverse load of $-140\,\text{MPa}$. (b) Transverse load of $-600\,\text{MPa}$.

6 | Conclusion

The critical currents derived from measurements conducted on DI-BSCCO tapes under transverse applied load, with a 1 mm pushing head all degrade irreversibly around $-250\,\mathrm{MPa}$.

The samples measured with a 2 mm pushing head show no degradation at $-250\,\mathrm{MPa}$. It is suggested that the mechanical resistance against plastic silver stabilizer material relocation, which squeezed between the pushing head and anvil, is larger because of the larger volume and distance at a 2 mm width head.

Therefore a method is followed to scale the pushing head sexperimental results to the more homogeneous Flutter coil load condition. The 3D simulation results of the experiment yields a similar failure curvature as the stress-critical current-curves found from the experiment. From this, a failure criterion for the BSCCO filaments of $\sigma_3 = -775\,\mathrm{MPa}$ was determined. The rule of mixtures approximation, which was used in the 3D model, has been validated in the 2D model.

A single tape inside the Flutter coil has been modeled and with the previously found failure criterion, the point of failure of the coil is determined. The transverse limit of the coil amounts to $-600\,\mathrm{MPa}$. The coil under full operational load reaches a maximum transverse load of approximately $-140\,\mathrm{MPa}$. This means that under full load the safety margin is approximately 300%.

7 | Recommendation

The displacement of the material along the x-axis (figure 5.10), needs to be compared to simulations with other pushing head widths in future work. Whilst doing this, an other setup to handle larger forces could also be made. This would allow the irreversible degradation to be visible for larger pushing head widths.

The coil has been evaluated by simulating a single tape inside the Flutter coil and approximating all tapes as equal. So in future research a slice of the coil could be taken to view the homogeneity of the winding pack and check if any irregularities changes the limits of the coil significantly.

Acknowledgement

First of all would like to thank my supervisor Arend Nijhuis, for the time and effort he has put in during the course of my thesis.

Secondly I would like to thank Arno Godeke, for showing me a different perspective on certain parts of my thesis.

Now I want to say thanks to Jaap, Jeroen, Gonçalo (A.K.A. Portugoose) and Keyang for helping me out with COMSOL Multiphysics®, which was a huge help and saved me a lot of time.

I would like to acknowledge my colleagues from EMS for the wonderful time. I want to say special thanks to Ruben and Cris (A.K.A. Sea Farlake). "Het kan ook niet normaal" with us. We have had so much laughter together, whether it was playing tennis or just Cris marching into our office whilst shouting "PRUTSERS!" in the hope that someone is in an meeting.

Lars deserves a special place in this chapter. He supported me, pulled me out of my depression, we sport a lot together and if there is one person I'd blindly trust, it's him.

Outside of EMS my friends were always there to support me and to have good times with. Whether it was playing board games or "just one more game with Vayne", my feeding friends are always ready to make fun of me. A mate of me once said: "The moment your friends stop taking the piss out of you, is the moment they stop caring." And boy, they care a lot.

Last but not least, my family. They provided a good environment throughout my study and thesis. This is not a given for everyone and I'm happy and grateful to have them.

References

[1] A. Godeke, L. Alberty, E. Akcöltekin, R. Babouche, C. Detourbe, R. Nast, C. Radermacher, H. Röcken, A. Roth, M. Schillo, P. vom Stein, M. Walpole, J. Wittschen, K. Hayashi, E. Shizuya, H. J. G. Krooshoop, R. Lubkemann, A. Nijhuis, C. H. Vermeer, W. A. J. Wessel, J. Krause, J. Wiezoreck, A. Otto, and L. Saraco, "Research at varian on applied superconductivity for proton therapy," *Superconductor Science and Technology*, vol. 33, p. 064001, apr 2020.

[2] C. Inc., "Comsol multiphysics reference manual, version 5.5," 2021. COMSOL Inc.

[3] D. van Delft and P. Kes, "The discovery of superconductivity," *Physics Today*, vol. 63, no. 9, pp. 38–43, 2010.

[4] S. C. Wimbush and N. M. Strickland, "A public database of high-temperature superconductor critical current data," *IEEE Transactions on Applied Superconductivity*, vol. 27, no. 4, pp. 1–5, 2017.

[5] N. Ayai, T. Kato, J. Fujikami, K. Fujino, S. Kobayashi, E. Ueno, K. Yamazaki, M. Kikuchi, K. Ohkura, K. Hayashi, K. Sato, and R. Hata, "DI-BSCCO wires by controlled over pressure sintering," *Journal of Physics: Conference Series*, vol. 43, pp. 47–50, jun 2006.

[6] L. B. Valdes, "Resistivity measurements on germanium for transistors," *Proceedings of the IRE*, vol. 42, pp. 420–427, Feb 1954.

[7] S. L. Bray, J. W. Ekin, C. C. Clickner, and L. J. Masur, "Transverse compressive stress effects on the critical current of bi-2223/ag tapes reinforced with pure ag and oxide-dispersion-strengthened ag," *Journal of Applied Physics*, vol. 88, no. 2, pp. 1178–1180, 2000.

[8] S. Ito and H. Hashizume, "Transverse stress effects on critical current and joint resistance in mechanical lap joint of a stacked hts conductor," *IEEE Transactions on Applied Superconductivity*, vol. 22, no. 3, pp. 6400104–6400104, 2012.

[9] T. Takao, T. Ito, K. Umekawa, Y. Fukasawa, H. Tanaka, and M. Umeda, "Influence of compressive length of normal stress on degradation in bi-2223 tapes," *IEEE Transactions on Applied Superconductivity*, vol. 15, no. 2, pp. 2488–2491, 2005.

[10] K. Umekawa, T. Ito, T. Takao, H. Tanaka, and M. Umeda, "Transversal compressive force and superconducting transition properties of bi-2223 tapes," *Physica C: Superconductivity*, vol. 401, no. 1, pp. 251–254, 2004. Proceedings of the International Cryogenic Materials Conference: Topical Conference on the Voltage-Current Relation in Technical Superconductors.

[11] S. S. Oh, D. W. Ha, H. S. Ha, C. Park, Y. K. Kwon, K. S. Ryu, and H. S. Shin, "Influence of transverse compressive stress onIcdegradation of ag alloy sheathed bi-2223 tapes," *Superconductor Science and Technology*, vol. 17, pp. 130–134, nov 2003.

[12] J. Ekin, *Experimental Techniques for Low-Temperature Measurements: Cryostat Design, Material Properties and Superconductor Critical-Current Testing*. Oxford: Oxford University Press, 2006.

[13] R. L. Holtz, "Transverse mechanical properties of bscco/ag multifilamentary tapes," *IEEE Transactions on Applied Superconductivity*, vol. 11, no. 1, pp. 3238–3241, 2001.

[14] M. Sugano, K. Osamura, and A. Nyilas, "Analysis of stress–strain behavior in bi2223 composite tapes," *Physica C: Superconductivity*, vol. 412-414, pp. 1114–1119, 2004. Proceedings of the 16th International Symposium on Superconductivity (ISS 2003). Advances in Superconductivity XVI. Part II.

[15] H. Kitaguchi, J. Nishioka, T. Hasegawa, K. Itoh, H. Kumakura, K. Togano, and H. Wada, "Effects of strain on the critical current of bi-2223/ag tapes," *IEEE Transactions on Applied Superconductivity*, vol. 12, no. 1, pp. 1141–1144, 2002.

[16] A. Otto, E. Podtburg, R. Mason, and P. Antaya, "Advances in the brass and stainless steel reinforcement of high temperature superconducting wires," *IEEE Transactions on Applied Superconductivity*, vol. 17, no. 2, pp. 3071–3074, 2007.

[17] N. Ayai, K. Yamazaki, M. Kikuchi, G. Osabe, H. Takaaze, H. Takayama, S. Kobayashi, J. Fujikami, K. Hayashi, K. Sato, K. Osamura, H. Kitaguchi, S. Matsumoto, T. Kiyoshi, and J. Shimoyama, "Electrical and mechanical properties of di-bscco type ht reinforced with metallic sheathes," *IEEE Transactions on Applied Superconductivity*, vol. 19, pp. 3014–3017, June 2009.

[18] K. Osamura, S. Machiya, and G. Nishijima, "Reversible stress and strain limits of the critical current of practical REBCO and BSCCO wires," *Superconductor Science and Technology*, vol. 29, p. 094003, jul 2016.

[19] K. Osamura, S. Machiya, T. Kawasaki, S. Harjo, T. Kato, S. Kobayashi, and G. Osabe, "Mechanical—electromagnetic property of stainless sheet laminated BSCCO–2223 wires," *Materials Research Express*, vol. 6, p. 026001, nov 2018.

[20] D. Fabiani and G. C. Montanari, "Short-term and long-term mechanical characteristics of bscco steel-reinforced tapes," *IEEE Transactions on Applied Superconductivity*, vol. 14, no. 3, pp. 2015–2021, 2004.

[21] M. Hojo, K. Osawa, T. Adachi, Y. Inoue, K. Osamura, S. Ochiai, N. Ayai, and K. Hayashi, "Effect of fatigue loading on critical current in stainless steel-laminated di-bscco superconducting composite tape," *Physica C: Superconductivity and its Applications*, vol. 470, no. 20, pp. 1373 – 1376, 2010. Proceedings of the 22nd International Symposium on Superconductivity (ISS 2009).

[22] Z. Lu, X. Huang, Y. He, J. Li, J. Sun, Y. Wang, X. Zong, J. Wang, L. Chen, C. Li, P. Zhang, Y. Feng, and L. Zhou, "Axial tensile and compressive strain effects on the critical current of bi-2223 superconducting tapes," *Physica C: Superconductivity*, vol. 386, pp. 158–161, 2003. Proceedings of the topical conference of the International Cryogenic Materials Conference (ICMC 2002). Superconductors for Practical Applications.

[23] C. Li, E. Mossang, B. Bellin, A. Antonevici, and P. Zhang, "Effects of compressive stress on the critical current of bi-2223 tapes," *Physica C: Superconductivity and its Applications*, vol. 463-465, pp. 882–884, 2007. Proceedings of the 19th International Symposium on Superconductivity (ISS 2006).

[24] T. Megson, *Structural and Stress Analysis*. Elsevier, 1996.

[25] M. Ahoranta, J. Lehtonen, and T. Tarhasaari, "Finite element models for thermal stress, axial tension, bending, and transversal compression of filamentary bi-2223 tapes," *Superconductor Science and Technology*, vol. 22, no. 1, p. 015012, 2008.

[26] `https://conference-indico.kek.jp/event/62/contributions/1247/attachments/839/881/KEK_Workshop201901_hayashi.pdf`. [Online; accessed April-22-2021].

[27] E. Ueno, T. Kato, and K. Hayashi, "Race-track coils for a 3 mw hts ship motor," *Physica C: Superconductivity and its Applications*, vol. 504, pp. 111–114, 2014.

[28] N. Bay and M. Nielsen, "Mechanical processing of ag/bscco high temperature superconductor tape," *Journal of Materials Processing Technology*, vol. 151, no. 1, pp. 18–26, 2004. Special Volume dedicated to Professor Z.R. Wang on the occasion of his 70th Birthday.

[29] `https://global-sei.com/super/hts_e/guide.html`. [Online; accessed May-7-2019].

[30] S. Otten. personal communication. [August-9-2021].

[31] R. R. Gomatam and E. Sancaktar, "A comprehensive fatigue life predictive model for electronically conductive adhesive joints under constant-cycle loading," *Journal of Adhesion Science and Technology*, vol. 20, no. 1, pp. 87–104, 2006.

[32] M. A. Chowdhury, D. M. Nuruzzaman, B. K. Roy, A. Islam, Z. Hossain, and M. R. Hasan, "Experimental investigation of friction coefficient and wear rate of stainless steel 202 sliding against smooth and rough stainless steel 304 counter-faces," *Friction and wear research*, vol. 1, no. 3, pp. 34–41, 2013.

[33] Y. Huo and C. C. Lee, "The growth and stress vs. strain characterization of the silver solid solution phase with indium," *Journal of Alloys and Compounds*, vol. 661, pp. 372–379, 2016.

[34] I. A. Parinov, *Microstructure and Properties of High-Temperature Superconductors*. Berlin, Heidelberg: Springer Berlin Heidelberg, 2012.

[35] "Dupont™ kapton® hn polyimide film." `https://www.dupont.com/content/dam/dupont/amer/us/en/products/ei-transformation/documents/DEC-Kapton-HN-datasheet.pdf`. [Online; accessed August-9-2021].

[36] "Ctd-101k epoxy resin system," 2014. Data Sheet (Lafayette, CO: Composite Technology Development).

[37] R. Bossert, S. Krave, G. Ambrosio, N. Andreev, G. Chlachidze, A. Nobrega, I. Novitski, M. Yu, and A. Zlobin, "Recent progress and tests of radiation resistant impregnation materials for nb 3 sn coils," in *AIP Conference Proceedings*, vol. 1574, pp. 132–139, American Institute of Physics, 2014.

[38] J. W. Gooch, *Law of Mixtures*, pp. 421–421. New York, NY: Springer New York, 2011.

[39] ECO5, "Update – flutter coil modeling varian purchase order #7060107 (eco5: P16)," February 2019. Presentation.

List of Figures

List of Tables

Appendices

A | Savety

Liquid nitrogen is used to cool the sample down, which needs to be handled with care. The liquid nitrogen can cause extensive tissue damage or burns, when the skin comes into contact with the liquid. This will happen when the leidenfrost effect has worn off. The nitrogen will also cool the setup and the siphon. Both of those are made of solids with a higher thermal conductivity than nitrogen gas, so even more care needs to be taken when handing these.

Another concern with liquid nitrogen is the ability of displacing oxygen in the air. Even up to a point where the oxygen present does no longer support human life. This can cause dizziness, loss of consciousness and even death. These tell tell signs are hard to recognize since the lowered oxygen level will reduce the ability to judge the situation.

The liquid is transported in dewars. These dewars can be closed for transportation and to build up pressure for filling a cryostat for example. Unintended pressure buildups can become a hazard. When opening the gas valve, a lot of cold nitrogen gas will come out under a lot of pressure. When the dewar is filled up to maximum capacity, it can happen that some liquid nitrogen will come out as well.

The work was carried out with all of these concerns in mind. When handling liquid nitrogen, safety glasses and cryogenic gloves were used. To make sure there is a good supply of oxygen, the air change rate in the lab is at least 7. Then there is the pressure concern. All dewars have an overpressure valve, this one is not supposed to be used for everyday use, but it is there in case the normal valves have been closed and pressure builds up unintended. In the highly unlikely case that something does go wrong, there will always be someone nearby to assist.